Chapter IV

ENGINEERING THE DYNAMIC PROPERTIES OF PROTEIN HYDROGEL NETWORKS THROUGH SEQUENCE VARIATION

1. Abstract

Network dynamics control the viscoelasticity and erosion rate of materials and influence biological processes at multiple length scales. In hydrogel networks prepared from recombinant artificial proteins, dynamic behaviors such as stress relaxation and energy dissipation can arise from the transient intermolecular association of protein domains that form physical network junctions. In this chapter, variation of the protein sequence is explored as a strategy to tune the characteristic relaxation timescale of protein networks. Single point mutations to coiled-coil physical cross-linking domains that associate within an end-linked covalent network can alter the characteristic relaxation time over five orders of magnitude as demonstrated by dynamic oscillatory shear rheology experiments and stress relaxation measurements. Using a pair of orthogonal coiled-coil physical cross-linking domains, networks with two distinct relaxation timescales were also engineered. This work demonstrates how the time-dependent response of a polymeric material to mechanical deformation can be encoded within the sequence of a polymer.

2. Introduction

Cellular behaviors such as proliferation [1], spreading and migration [2], and differentiation [3] are regulated in part by the stiffness of the local tissue microenvironment. These observations have led to considerable efforts to design materials with tunable mechanical properties for applications in tissue engineering and for fundamental research of mechanotransduction. The stiffness or compliance of biomaterials is typically characterized by an elastic modulus relating the deformation and stress at small strains. The moduli of materials used in cell culture can vary from less than 1 kPa for soft gels [4] to more than 1 GPa for glass and tissue culture polystyrene [5]. Several recent studies have suggested that in addition to the elasticity of a material, its viscous or dissipative properties may also influence cellular behavior [6-8]. To better understand these phenomena and to potentially harness them for cell and tissue engineering applications, it will be necessary to develop materials with tunable dynamic properties.

Dynamic materials have been engineered from both synthetic polymers and proteins. Examples of dynamic synthetic polymer networks include viscoelastic gels and elastomers cross-linked by hydrophobic interactions [9], hydrogen bonds [10], metal-ligand complexes [11-14], and dynamic covalent bonds [15, 16]. Stress relaxation and energy dissipation in these materials arise from the transient nature of at least some of the network junctions, and the characteristic relaxation timescales can therefore be tuned by modifying the lifetime of the transient cross-links. In protein hydrogel networks, dynamic properties likewise emerge from transient physical cross-links between associating domains on neighboring protein chains. Examples of dynamic physical cross-linking domains in artificial proteins include α-helical coiled coils [17-20] and collagen-like triple helices [21].

Hydrogels cross-linked by coiled-coil domains are the best-studied example of dynamic protein networks, and engineering the sequence the cross-linking domains in these proteins is a potential strategy to program the dynamic viscoelastic behavior of these materials. Using a pH-responsive leucine zipper coiled coil, Shen *et al*. showed that the lifetime of a physical cross-link is related to the characteristic strand exchange time (τ_e), or the exchange rate of a strand between different coils. Although exchange times have only been reported for a small number of coiled coils derived from transcription factors, structural proteins, and designed peptides, these measurements reveal a large dynamic range that may be useful for engineering the relaxation behavior of protein-based materials [18, 22-25]. In these coiled coils, τ_e varied from approximately 1 s to greater than 10^4 s. This large dynamic range might reflect the diverse roles of coiled coils in biological systems. For example, coiled coils that mediate the dimerization of transcription factors such as Fos and Jun may require a very fast exchange rate ($\tau_e < 10$ s) to allow a cell to rapidly alter its transcriptional program [25]. Tropomyosin coiled coils, however, are much more stable ($\tau_e \approx$ 500 to >20,000 s) [22]. Coiled-coil dynamics are also sensitive to pH [18], allosteric regulation by binding partners [25], and mutation of the amino acid sequence [24]. The effects of mutations within coiled coil domains on the characteristic exchange time are particularly intriguing as this might allow the relaxation behavior of protein networks to be encoded within the protein sequence.

In this work, a set of seven artificial proteins was prepared that differ only by the identity of the side chain at one residue within a helical domain (P) that associates to form coiled coils. Association of these domains within an end-linked hydrogel network results in transient physical cross-linking and viscoelastic behavior. These networks were characterized by dynamic oscillatory rheology and stress relaxation experiments in order to measure a characteristic relaxation time for each material. Building on this strategy, hydrogel networks with more complex dynamic behavior

were then prepared from mixtures of two artificial proteins. The results described in this chapter demonstrate that the macroscopic dynamic behavior of a protein network can be encoded at the level of the primary sequence and show that very small changes to a single amino acid reside can have significant effects on the macroscopic length scale.

3. Materials and Methods

3.1 Site-Directed Mutagenesis and Cloning of Artificial Protein Genes

EPE variants were generated by site-directed mutagenesis of the sequence encoding the P domain on a pUC19 plasmid (pUC19 P) using oligonucleotides reported in Appendix A. After sequencing to confirm the correct mutant was obtained, the resulting pUC19 P-*mutant* plasmids (pUC19 P T40A, pUC19 P Q54A, pUC19 P I58A, pUC19 P L37A, pUC19 P L37V, pUC19 P L37I) were digested with *SacI* and *SpeI* (New England BioLabs, Ipswich, MA) to isolate the fragments encoding P-*mutant*. The residue numbering convention is based on the amino acid sequence of rat cartilage oligomeric matrix protein (COMP), from which the P domain is derived [26]. The excised fragments were ligated into the pQE-80L EPE plasmid (described in Chapter 3) that was digested with the same enzymes. This replaces the original P domain with the mutated variant. Site-directed mutagenesis was not carried out directly on pQE-80L EPE due to difficulties created by the highly-repetitive, GC-rich elastin-like domains. Chemically competent BL21 *Escherichia coli* (New England BioLabs) were transformed with the pQE-80L EPE-*mutant* plasmids (pQE-80L EPE T40A, pQE-80L EPE Q54A, and pQE-80L EPE I58A, pQE-80L EPE L37A, pQE-80L EPE L37V, pQE-80L EPE L37I) for protein expression. The gene sequence and amino acid sequence of each protein are listed in Appendix A.

The pQE-80L EAE plasmid was constructed by subcloning the sequence encoding the A domain from pQE-9 PC10A [27] into the pQE-80L EPE plasmid in place of the sequence encoding the P domain. The forward primer (Appendix A) contained a *Sac*I overhang while the reverse primer bound the plasmid downstream of an in-frame *Spe*I site flanking the A domain in pQE-9 PC10A. The amplicon was digested with these enzymes and ligated into the pQE-80L EPE plasmid in place of P. The BL21 strain was also used for expression of EAE.

3.2 Protein Expression and Purification

Recombinant expression and purification of EPE, EAE, and the EPE variants is similar to the protocol described in Chapter 2 and Appendix B. Briefly, 1 L cultures were grown at 37 °C in Terrific broth containing 100 μg mL^{-1} ampicillin (BioPioneer, San Diego, CA) to an optical density at 600 nm (OD_{600}) of 1. Isopropyl β-D-1-thiogalactopyranoside (IPTG) (BioPioneer) was added to a final concentration of 1 mM and the cells were harvested 4 hr later by centrifugation at 6,000 *g* for 8 min at 4 °C. The cells were frozen at a concentration of 0.5 g mL^{-1} in TEN buffer (50 mM Tris, 1 mM EDTA, 100 mM NaCl, pH 8.0) supplemented with 5% (v/v) glycerol, 0.1% (w/v) sodium deoxycholate, and 0.1% (v/v) TritonX-100. After thawing, the lysate was treated with 10 μg mL^{-1} DNase I (Sigma, St. Louis, MO), 5 μg mL^{-1} RNase A (Sigma), 5 mM $MgCl_2$, and 1 mM phenylmethylsulfonyl fluoride (Gold Biotechnology, Olivette, MO) while shaking at 37 °C, 250 rpm for 30 min. The lysate was then sonicated for 5 min (2" on, 2" off, 30% power amplitude) (QSonica, Newton, CT) and allowed to rest for 2 hr on ice. β-mercaptoethanol (βME) (Sigma) was added to the lysate to a final concentration of 1% (v/v) following sonication.

The target proteins were purified from the *E. coli* lysate by three rounds of temperature cycling. The lysate was centrifuged at 39,000 *g* for 1 hr at 4 °C to remove insoluble proteins and cellular debris. Crystalline NaCl was added to the supernatant at a final concentration of 2 M followed by shaking at 250 rpm, 37 °C for 1 hr. The aggregated proteins were collected by centrifugation at 39,000 *g* for 1 hr at 37 °C and solubilized overnight at 4 °C at a concentration of 100 mg mL^{-1} in cold TEN buffer containing 1% (v/v) βME. Two more cycles were completed with 30 min centrifugation spins. The βME was omitted in the final resuspension step. Instead, 5 mM tris(hydroxypropyl)phosphine (THP) (Santa Cruz Biotechnology, Dallas, TX) was added and the protein solution was incubated at 4 °C for 2 hr. The purified protein was desalted into LC-MS grade water (Sigma) using Zeba 7K MWCO columns (Thermo Fisher Scientific, Waltham, MA) and lyophilized for 4 days. The lyophilized protein was stored under argon at -80 °C or used immediately.

3.3 Protein Characterization by SDS-PAGE, ESI-MS, and Ellman's Assay

Fractions were saved from each step in the temperature cycling purification. Proteins were extracted from the pelleted fractions with a volume of 8 M urea equal to the volume of the supernatant from that step. These solutions were then diluted with an equal volume of water to adjust the final urea concentration to 4 M. Samples of the supernatant were diluted with an equal volume of 8 M urea to obtain a final urea concentration of 4 M. All of the fractions were then mixed with 2x SDS loading buffer containing 5% (v/v) βME and boiled for 10 min before loading 2 μL per well in a 15 well, Novex NuPage 4-12% Bis-Tris SDS PAGE gel (Thermo Fisher Scientific). The gel was run in MES/SDS running buffer (Boston BioProducts, Ashland, MA) for

45 min at 180 V, fixed, and stained with colloidal blue protein staining solution (Life Technologies, Carlsbad, CA). Gels were imaged on a Typhoon Trio (GE Healthcare, Pittsburgh, PA).

Protein solutions (0.2 mg mL^{-1} in 0.1% formic acid) were analyzed by LC-MS using a Waters UPLC/LCT Premier XE TOF mass spectrometer (Waters, Milford, MA) by electrospray ionization in the positive ion mode with a MassPREP Micro desalting column. The mass spectrometer was calibrated with NaI using standard procedures and calibration was subsequently verified by running a standard solution of myoglobin. The mass spectrometer settings were: capillary voltage = 2.8 kV, cone voltage = 40, source temperature = 120 °C, and desolvation temperature = 350 °C, desolvation gas = 750 L hr^{-1}, acquisition range = 500 to 2000 in V mode, ion guide = 5. The mobile phase consisted of a gradient of water and acetonitrile with 0.1% formic acid. Electrospray mass spectra were deconvoluted using MaxEnt1 software.

The free thiol content of each protein was measured using Ellman's assay as described in Chapter 2 and Appendix B. Lyophilized proteins were dissolved in reaction buffer (100 mM sodium phosphate, 1 mM EDTA, pH 8) at a concentration of 5 mg mL^{-1}. The protein solution (250 μL) and Ellman's reagent (Sigma) stock solution (50 μL of 5 mg mL^{-1} reagent in reaction buffer) were added to 2.5 mL of reaction buffer. After 15 min incubation, the absorbance at 412 nm was measured on a Cary 50 UV/Vis spectrophotometer. The concentration of thiol groups was calculated from the absorbance value and the extinction coefficient 14,150 M^{-1} cm^{-1}.

The free thiol content was also estimated by non-reducing SDS-PAGE. Samples prepared for thiol quantitation by Ellman's assay were diluted 1:10 in SDS loading buffer, and 2 μL of each solution was loaded in a 15-well, Novex NuPage 4-12% Bis-Tris gel. Control lanes contained samples that were reduced by boiling in the presence of 5% (v/v) βME for 5 min. The gel was run in MES/SDS running buffer at 180 V for 45 min. Proteins were visualized with InstantBlue protein

stain (Expedion, San Diego, CA). The intensity of each band on the protein gel was quantified using ImageQuant software (GE Healthcare).

3.4 Hydrogel Cross-linking and Swelling

Lyophilized artificial proteins were dissolved at a concentration of 150 mg mL^{-1} in degassed cross-linking buffer (0.1 M sodium phosphate, 6 M guanidinium chloride, 0.4 M triethanolamine, pH 7.4) by sonicating for 2 min in an ultrasonic bath. Bubbles were removed by centrifugation at 10,000 *g* for 1 min. The PEG-4VS cross-linker was dissolved at a concentration of 150 mg mL^{-1} in degassed 0.4 M triethanolamine, pH 7.4. Cross-linking was initiated by mixing the two solutions at a volumetric ratio that gave a 1:1 stoichiometry between the thiol and vinyl sulfone functional groups. The solution was vortexed to ensure homogeneous mixing and quickly pipetted onto a glass slide that was treated with SigmaCote (Sigma). A second treated glass slide was placed on top of the droplet separated by spacers cut from a 1 mm rubber sheet (McMaster-Carr, Santa Fe Springs, CA). The slides were clamped together and the gels were allowed to cure in the dark overnight at ambient temperature.

Hydrogels prepared for rheological measurements were transferred to a dish containing 6 mL of PBS (pH 7.4) containing 6 M guanidinium chloride (GndCl). The gels were swollen in this buffer for three hours before switching to PBS with 3 M GndCl for 3 hr, then PBS with 2 M GndCl for 3 hr, PBS with 1 M GndCl for 3 hr, and finally PBS. The gradual decrease in the guanidinium concentration is designed to allow unreacted protein chains to diffuse out of the gel and to promote proper folding of the coiled-coil domains.

For swelling experiments, hydrogels were transferred to 6-well plates containing 3 mL of PBS plus 6 M GndCl per well. The gels were swollen to equilibrium and the swollen mass was measured after 48 hr. The guandinium concentration was gradually decreased from 6 M to 0 M in PBS as described above. Swollen masses were recorded for gels in PBS after 48 hr of swelling followed by washing the gels at least five times with ddH_2O over the course of 72 hr to remove the salts. The dry mass was obtained after lyophilization. The mass swelling ratio Q_m was calculated for PBS with 6 M guanidinium chloride and PBS by dividing the swollen mass for each condition by the dry mass of the network. For extended swelling in PBS longer than 1 day, 0.02% (w/v) sodium azide (Sigma) was added to the buffer to inhibit microbial contamination.

3.5 Rheological Characterization of Protein Hydrogels

Swollen hydrogels prepared from EPE, EAE, and EPE variants were characterized by small amplitude oscillatory shear rheology and shear stress relaxation on an ARES-RFS strain-controlled rheometer (TA Instruments). Gels were cut into disks with an 8 mm biopsy punch (Miltex) and loaded between the 8 mm parallel plate test geometry as described in Chapters 2 and 3 and Appendix B. Frequency sweeps were acquired at 2% strain amplitude, 25 °C. Following the frequency sweep, a stress relaxation experiment was performed with a 2% step strain at 25 °C.

4. Results and Discussion

4.1 Protein Design, Synthesis, and Characterization

To explore the role of protein sequence on the relaxation dynamics of protein networks, six variants of the EPE protein described in Chapter 3 were designed, each containing a single

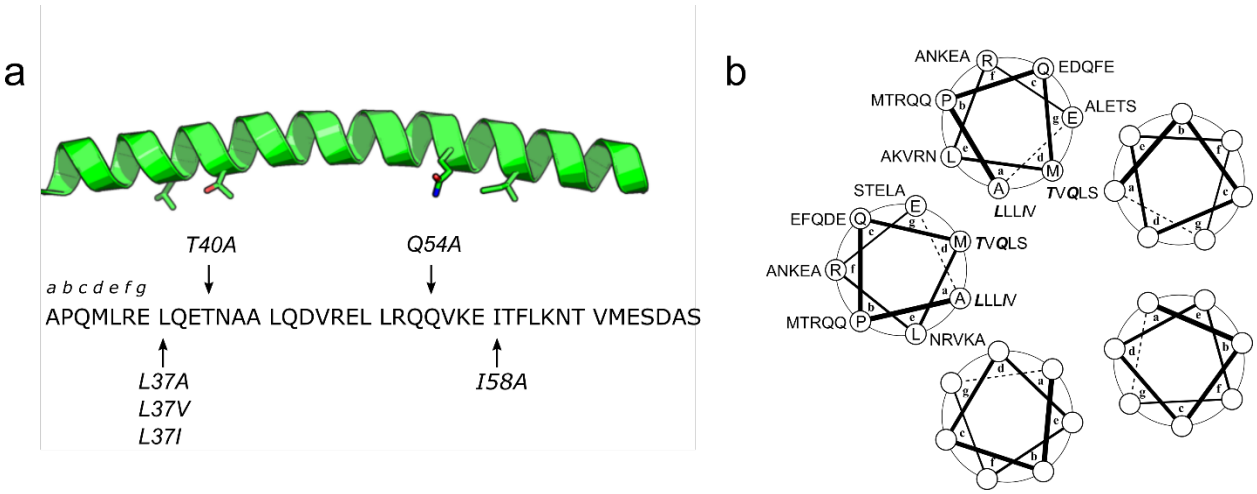

Figure IV-1. Point mutations within the P helical domain. (**a**) The midblock domain P in EPE forms a helical structure when associated in a homopentameric coiled coil (PDB 1VDF from ref. [32]). Below the structure, the amino acid sequence of the P domain is divided into six heptad repeats using the conventional *abcdefg* notation for coiled-coil peptides. The mutated residues leucine 37, threonine 40, glutamine 54, and isoleucine 58 are noted with arrows. (**b**) The pentameric coiled coil can also be represented by a helical wheel diagram. The mutated residues shown in bold, italic type face.

point mutation located within the P midblock domain. The mutated residues were selected based on the work of Gunasekar *et al*., in which alanine scanning mutagenesis was performed on the *a* and *d* positions that comprise the coiled-coil interface [28]. Point mutations to alanine at one of several aliphatic residues in P (Leu37, Leu44, Val47, Leu51, or Ile58) resulted in destabilization of the helical structure while mutations of polar residues (Thr40 or Gln54) to alanine resulted in stabilization [28]. An increase in thermal stability was also observed when Gln54 was mutated to leucine [29] or isoleucine [30]. In Chapter 3, it was shown that hydrogels prepared by cross-linking an EPE variant containing the L44A mutation do not exhibit physical cross-linking, but the effects of other mutations that are stabilizing or less destabilizing than L44A on the behavior of chemical-physical networks are unknown.

The six EPE variants include EPE T40A and EPE Q54A, which are expected to form more stable coiled coils than EPE (referred to as wild-type or WT), and EPE I58A, which is expected to form less stable coiled coils than WT. The remaining three variants, EPE L37A, EPE L37V, and EPE L37I, contain point mutations at residue 37. Replacement of leucine 37 with alanine and valine, which have smaller aliphatic side chains, is expected to decrease coiled-coil stability. The effect of the L37I mutation on the stability of the coiled-coil is difficult to predict because the mutation results in only a small change to the branching structure of the aliphatic side chain. The positions of the point mutations within the P domain are shown in Figure IV-1.

EPE and its variants were expressed in *Escherichia coli* strain BL21 and purified by inverse temperature cycling (Figure IV-2). Typical yields exceeded 100 mg of purified protein per liter of culture. The proteins were reduced, desalted, and stored under inert atmosphere at -80 °C to ensure a high free thiol content, which was measured by Ellman's assay [31] to be between 83-91% for all EPE variants (Figure IV-3 and Table IV-1). The results of Ellman's assay were also consistent with analysis by non-reducing SDS-PAGE, which confirmed that the proteins were monomeric (Figure IV-4 and Table IV-2). The molecular weight of the proteins were confirmed by electrospray ionization mass spectrometry (ESI-MS) (Table IV-3).

4.2 Hydrogel Cross-linking and Swelling

Hydrogels were prepared by end-linking the artificial proteins with 4-arm poly(ethylene glycol) vinyl sulfone (PEG-4VS) as described in the previous chapters. Gels were prepared from each EPE variant in an identical manner, although slight variations may arise due to differences in the protein thiol content or purity. For all gels, the total polymer (protein and PEG-4VS)

concentration was 15 wt% during cross-linking and the stoichiometry of protein thiols to vinyl sulfone groups on PEG-4VS was nominally 1:1. After cross-linking, the gels were swollen in decreasing concentrations of guanidinium chloride (6M, 3M, 2M, 1M, 0M) in PBS to remove unreacted polymer and to promote refolding of the helical midblocks into coiled-coil cross-links. Hydrogels were swollen in PBS for at least 48 hr prior to either measurement of the swollen mass or rheological characterization. The mass swelling ratio (Q_m) for each hydrogel is plotted in Figure IV-5.

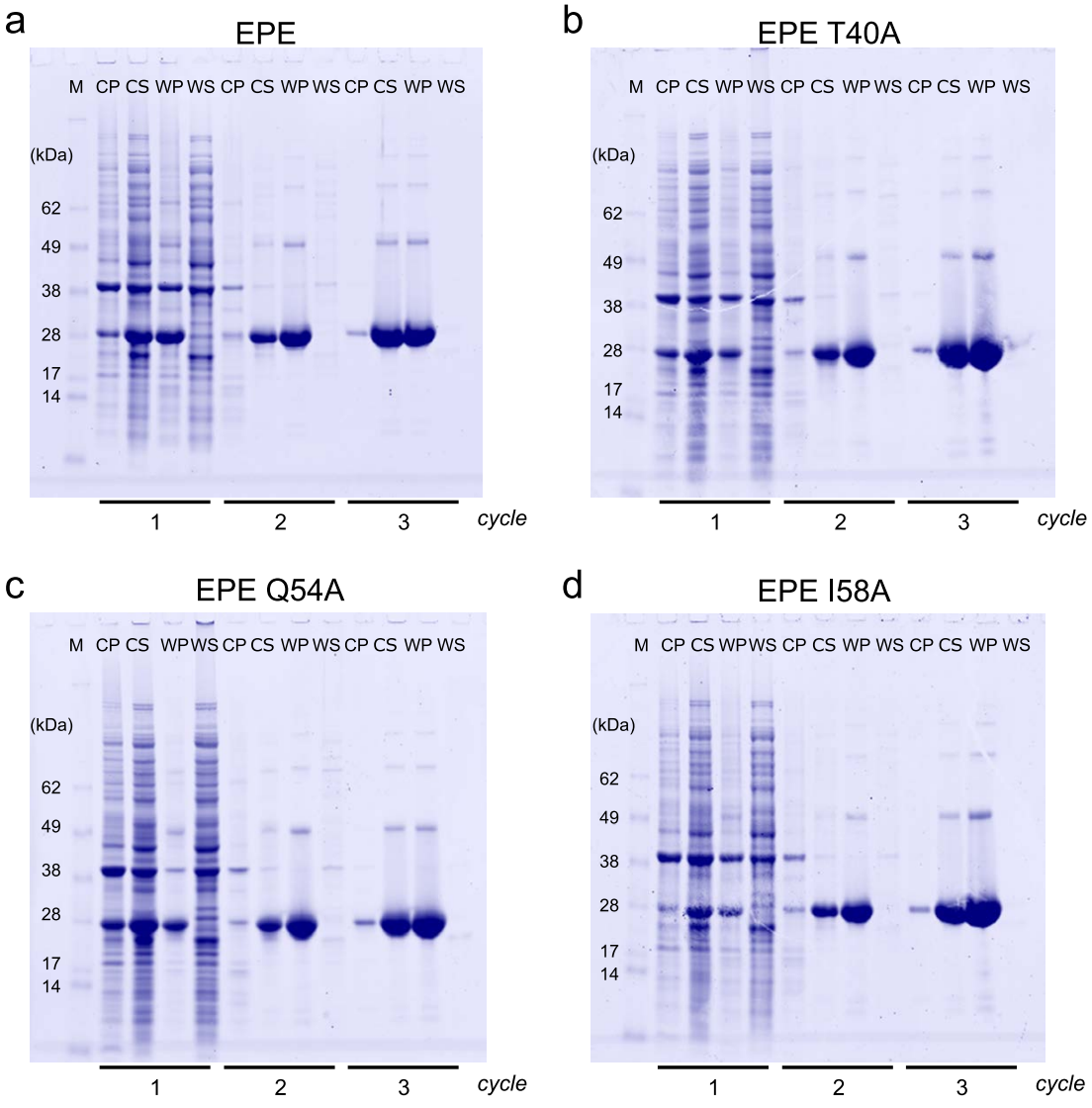

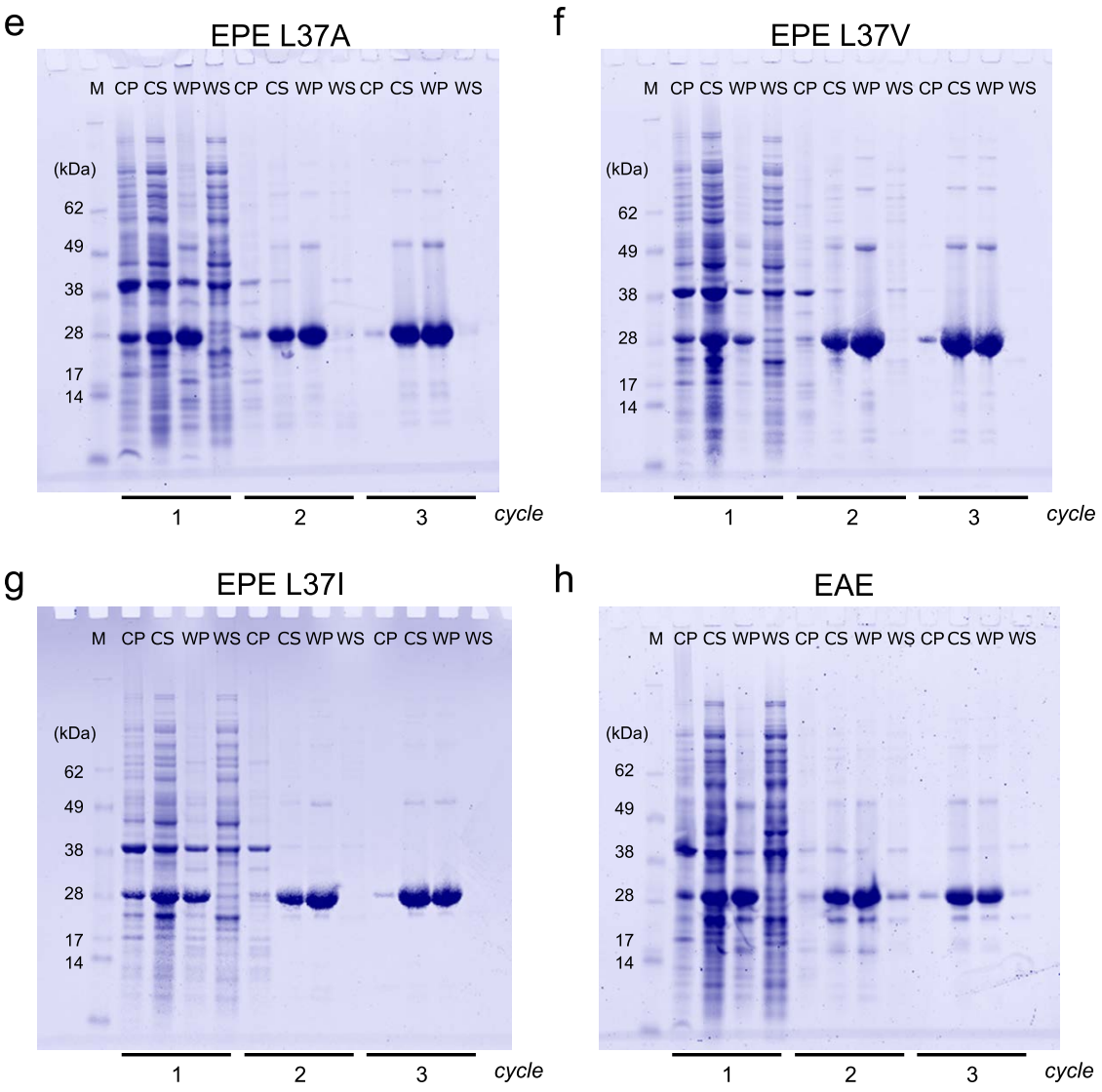

Figure IV-2 (begins on previous page). SDS PAGE analysis of inverse temperature cycling. Samples of each fraction were saved throughout the inverse temperature cycling purification. (**a-h)** EPE, EPE T40A, EPE Q54A, EPE I58A, EPE L37A, EPE L37V, EPE L37I, and EAE. Elastin-like proteins are soluble in the cold step of each cycle (4 °C, low ionic strength) and insoluble in the warm step of each cycle (37 °C, 2 M NaCl). Pure proteins were obtained after three cycles. The molar masses of the nine artificial proteins are nearly identical. Only EAE can be distinguished from the EPE variants on the basis of electrophoretic mobility. (Abbreviations: CP – cold pellet, CS – cold supernantant, WP – warm pellet, WS – warm supernatant, M – SeeBlue protein marker with molecular weights in kDa).

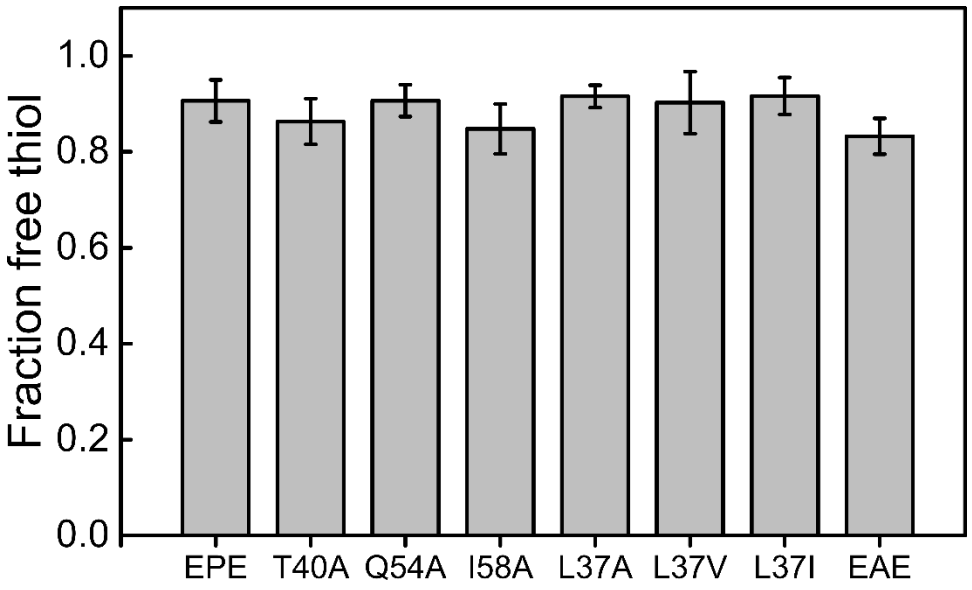

Figure IV-3. Ellman's assay quantitation of the free thiol content in artificial proteins. The fraction of free thiol groups was calculated by dividing the concentration of thiols measured by Ellman's assay by the expected concentration of thiols assuming that each protein chain contains two cysteine residues. The values all fall between 83% and 91%. Analysis of the proteins by non-reducing SDS-PAGE (Figure IV-4 and Table IV-1) suggest that deviations from the expected concentration of free thiols arise from the formation of intermolecular disulfides (dimers, trimers, etc.) and intramolecular disulfides (cyclized monomers and higher order species).

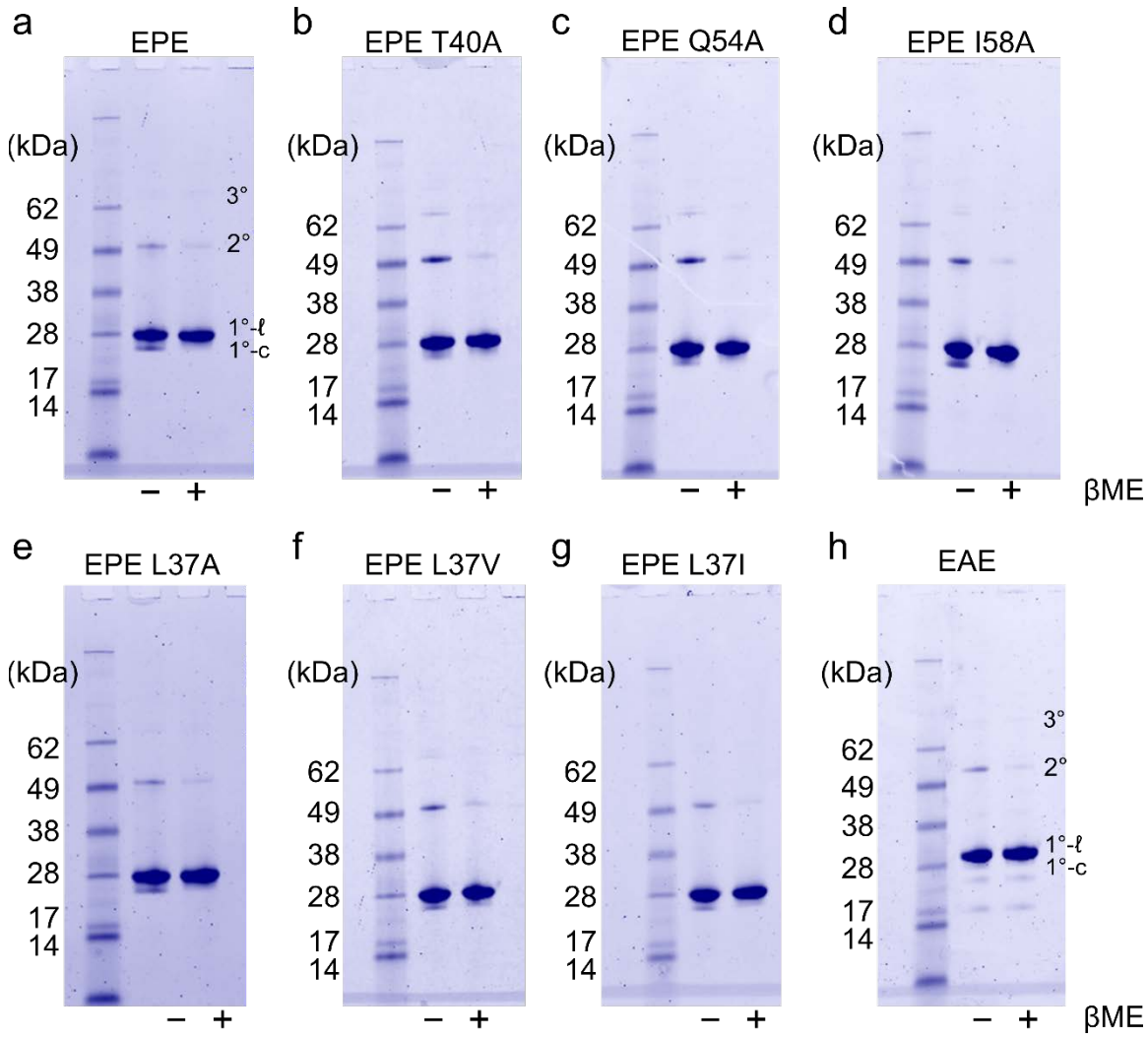

Figure IV-4. Analysis of protein oligomerization state by non-reducing SDS-PAGE. Each gel image contains three lanes. Lane 1: SeeBlue protein molecular weight marker with molecular weights (in kDa) of select bands labeled. Lane 2: artificial protein prepared in non-reducing buffer, denoted as "–" βME. Lane 3: artificial protein prepared in reducing buffer (with 5% (v/v) βME), denoted as "+" βME. In (**a**) and (**h**), the bands assigned as protein trimers (3°), dimers (2°), linear monomers (1°-ℓ), and cyclized monomers (1°-c) are labeled on the right-hand side of the gel. All artificial proteins are predominately monomeric and linear, although in general slightly more oligomers and cyclized monomers are present under non-reducing conditions (−) than in the reduced control lanes (+).

Protein	EPE	EPE L37A	EPE L37V	EPE L37I	EPE T40A	EPE Q54A	EPE I58A	EAE[a]
Trimer	<1	< 1	1	< 1	2	2	1	< 1
Dimer	6	5	9	7	15	14	11	7
Monomer (linear)	83	87	85	86	81	80	75	84
Monomer (cyclic)	9	8	5	7	2	5	12	4

[a] The EAE protein preparation has two small impurities that are likely degradation products. The integrated intensities of these bands on the SDS-PAGE gel were 3% and 2% of the total.

Table IV-1. Gel densitometry of protein bands in non-reducing SDS-PAGE. Lane profiles were created for the non-reducing sample lanes of the gel images in Figure IV-4. The intensities of bands assigned as linear monomers, cyclic monomers, dimers, and trimers in each lane were quantified by integrating the peak corresponding to each species. The data are reported as the percentage of the total area of all peaks detected in the lane.

Protein	EPE	EPE L37A	EPE L37V	EPE L37I	EPE T40A	EPE Q54A	EPE I58A	EAE
Ellman's assay	91	92	90	92	86	91	85	83
SDS-PAGE	86	90	90	90	89	87	81	88

Table IV-2. Percent free thiol by Ellman's assay and by non-reducing SDS-PAGE. The percentage of free thiol groups measured by Ellman's assay is compared to the percentage of free thiols calculated from the relative amount of each oligomer in the non-reducing SDS-PAGE gels (Figure IV-4 and Table IV-1). The data in Table IV-1 were multiplied by the expected number of free thiols per protein chain for each species (2 for linear monomers, 0 for cyclized monomers, 1 for dimers, and 2/3 for trimers). This value is then divided by 2, the expected number of thiols per chain if all proteins were in the reduced form.

EPE variant	Calculated mass	Observed mass
EPE	21,464	21,462
EPE T40A	21,434	21,434
EPE Q54A	21,407	21,406
EPE I58A	21,422	21,421
EPE L37A	21,422	21,423
EPE L37V	21,450	21,449
EPE L37I	21,464	21,462
EAE	21,908	21,909

Table IV-3. Protein mass determination by ESI-MS. Proteins were analyzed by LC-MS with electrospray ionization. The deconvoluted masses were all within 0.02% of the masses calculated from the protein sequences.

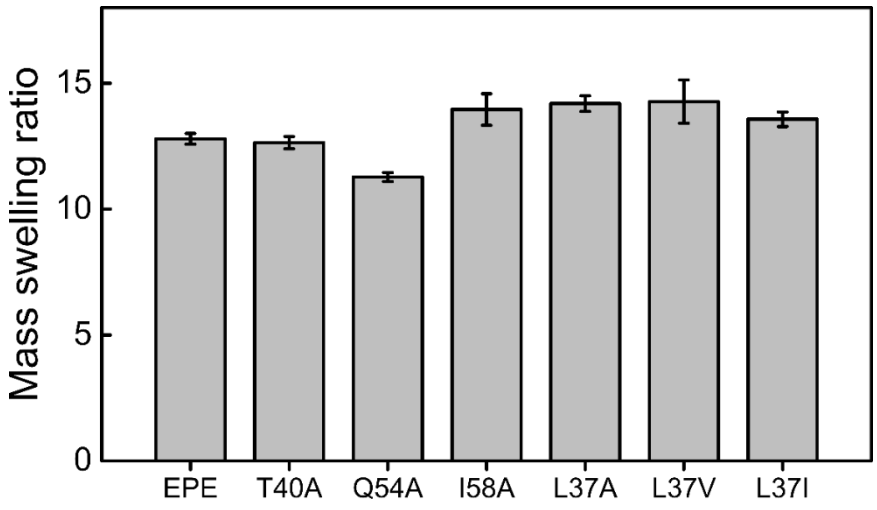

Figure IV-5. Equilibrium mass swelling ratio of hydrogels prepared from EPE and EPE variants. Hydrogels were swollen for 48 hr in PBS, pH 7.4 containing 0.02% (w/v) NaN_3 at ambient temperature.

4.3 Viscoelastic Behavior of EPE T40A, EPE Q54A, and EPE I58A Hydrogels

The rheological behavior of chemical-physical hydrogels prepared from EPE T40A, EPE Q54A, or EPE I58A was assessed by dynamic oscillatory rheology. In small amplitude oscillatory shear (SAOS) frequency sweep experiments (Figure IV-6 a), EPE T40A and EPE Q54A gels exhibit high frequency plateaus in *G'* that are similar in magnitude to the high frequency plateau observed with EPE gels. In these variants, however, the plateau behavior extends to lower frequencies than in EPE gels. Likewise, the maximum in *G"* also occurs at a lower frequency (0.003 rad s^{-1}) in EPE T40A gels. For hydrogels prepared from EPE Q54A, the maximum in *G"* was not observed in the experimental frequency range but likely occurs between 10^{-4} and 10^{-3} rad s^{-1}. In other words, the storage and loss modulus both appear to be shifted to lower frequencies compared to EPE. These observations are consistent with slower relaxation timescales for the coiled-coiled cross-linkers containing either the T40A mutation or the Q54A mutation. In hydrogels prepared from EPE I58A, the opposite behavior is observed. Both the transition zone between the plateaus in *G'* and the maximum in *G"* occur at higher values of ω, meaning that the relaxation of the physical cross-linking is faster in these materials. These experiments reveal a trend in the relaxation timescales of these materials (EPE Q54A > EPE T40A > EPE > EPE I58A) that is similar to the trend in the thermal stability measured by Gunaseker *et al* [28].

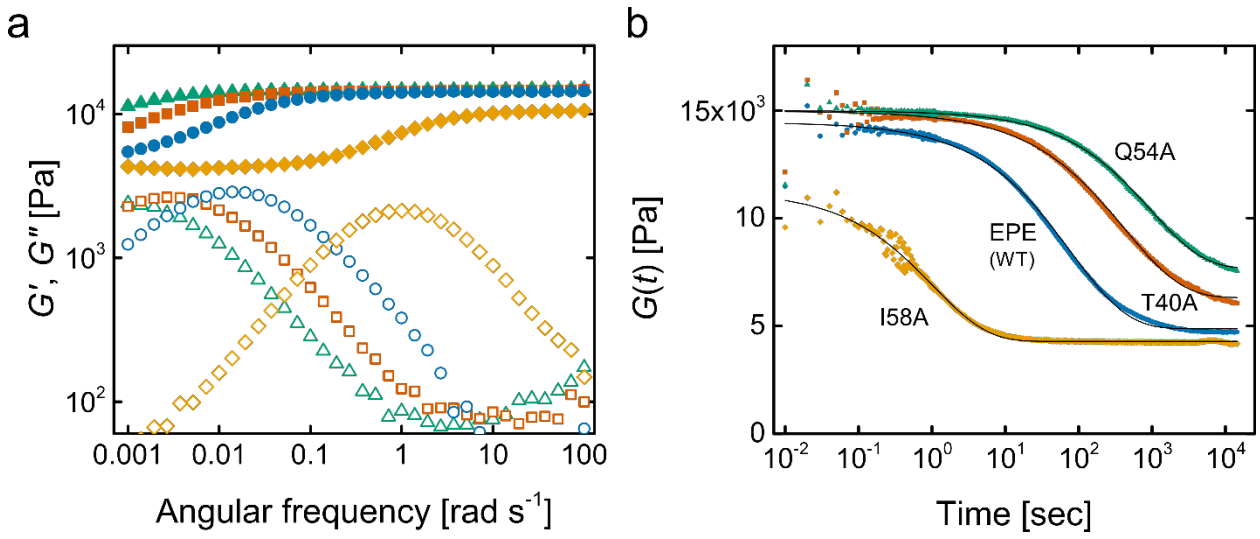

Figure IV-6. Rheology of EPE and variants EPE Q54A, EPE T40A, and EPE I58A. (**a**) Dynamic oscillatory frequency sweeps showing the storage modulus, (*G'*, filled symbols) and loss modulus (*G"*, open symbols) at 2% strain amplitude, 25 °C. In gels prepared from the EPE Q54A (triangles) and EPE T40A (squares) variants, the *G'* and *G"* curves are shifted to lower frequencies relative to EPE gels (circles). In gels prepared from the EPE I58A (diamonds) variant, the *G'* and *G"* curves are shifted to higher frequencies relative to EPE gels. (**b**) The same trend is observed in stress relaxation experiments in which gels were subjected to a 2% step strain at 25 °C. The characteristic relaxation times determined from the fitting the stretched exponential model (solid black lines) follow the trend $\tau_{Q54A} > \tau_{T40A} > \tau_{WT} > \tau_{I58A}$.

Because the dynamics of networks cross-linked by coiled-coil domains containing the T40A and Q54A mutations are too slow to observe the low frequency plateau behavior associated with the covalent network in the frequency sweep experiments, stress relaxation experiments were performed in which the gels were subjected to at a constant 2% strain for 4 hours (Figure IV-6 b). The relaxation function $G(t)$ was fit with the stretched exponential, or KWW, model previously used for physical protein hydrogels [19] and modified here with the parameter G_e to account for the presence of the permanent covalent network.

$$G(t) = G\exp\left(-\left(\frac{t}{\tau_{KWW}}\right)^{\beta}\right) + G_e \qquad \text{(Equation IV-1)}$$

The physical cross-linking is described by the parameter G as well as the relaxation timescale τ_{KWW} and the exponent β, which varies between 0 and 1. Calculation of a mean relaxation time, $\langle\tau\rangle$, for each material by Equation IV-2 confirmed the trend observed in the SAOS frequency sweeps.

$$\langle\tau\rangle = \frac{\tau_{KWW}}{\beta}\Gamma\left(\frac{1}{\beta}\right) \qquad \text{(Equation IV-2)}$$

($\Gamma\left(\frac{1}{\beta}\right)$ is the gamma function evaluated at β^{-1}.)

The mean relaxation time varied from approximately 1 second for EPE I58A gels to over 1500 seconds for EPE Q54A (Table IV-4). While this range is quite large considering the four materials differ by only a single amino acid side chain, the results are consistent with the strand exchange times measured for various coiled-coil systems. The more stable variants EPE Q54A and EPE T40A are slightly stiffer than EPE I58A and also slightly less swollen (Figure IV-5). Both observations can be explained by a greater fraction of folded P domains in the more stable variants, although differences in the amount of covalent cross-linking in each material arising from variations in the free thiol content or from the efficiency of the cross-linking reaction are also possible.

Protein	Mean Relaxation Time (s)
EPE L37A[a]	0.22 ± 0.13
EPE L37V	1.02 ± 0.14
EPE I58A	1.70 ± 0.15
EPE L37I	9.83 ± 1.19
EPE	134 ± 8
EPE T40A	762 ± 62
EPE Q54A	1608 ± 135

[a] EPE L37A was fit with a single exponential model

Table IV-4. **Characteristic relaxation times for EPE and the six single mutant variants.** The mean relaxation times were determined by fitting the stress relaxation data to the stretched exponential model in Eq. IV-1 and using the fitted parameters to evaluate Eq. IV-2.

The crystal structure of the P coiled-coil domain reported by Malashkevich *et al.* may provide some insight into the importance of the Thr40 and Gln54 positions [32]. The folded structure contains a pore along the entire coiled-coil axis. Although the buried residues are primarily hydrophobic, bound water molecules were observed near the hydroxyl side chain of Thr40 while a chloride ion is bound in an ion trap formed by the five Gln54 side chains (Figure IV-7). MacFarlane *et al*. suggested that water molecules in the hydrophobic pore allow the P domain to undergo dynamic opening or "breathing" motions in order to allow the entry of hydrophobic ligands such as all-*trans* retinol, vitamin D, and fatty acids [33-35]. In the native cartilage oligomeric matrix protein from which the P domain is derived, the coiled coil is stabilized by a C-terminal cysteine knot involving two cysteine residues from each chain [32]. The cysteine knot is not present in EPE or its variants as the cysteines were mutated to serine [27]. Therefore, the breathing motions that lead to channel opening in the knotted structure could lead to complete

dissociation of the physical cross-links in EPE hydrogels. The T40A and Q54A mutations may alter this process to produce less dynamic physical cross-linking, particularly if water or ion binding are altered in the mutant coils.

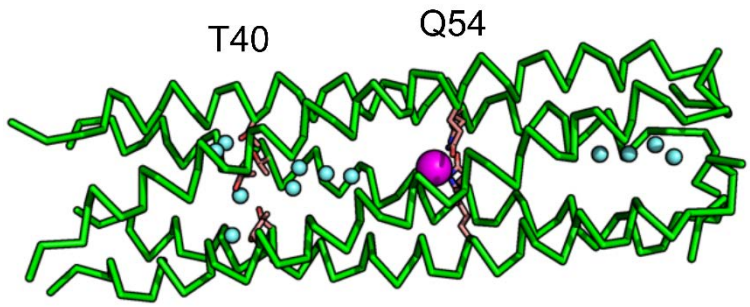

Figure IV-7. Structure of the P coiled coil pentamer. The five P strands are shown as green ribbons. Only the side chains of Thr40 and Gln54 are shown. Water molecules as depicted as light blue spheres, several of which are bound near Thr40. The chloride ion is depicted as a magenta sphere and is bound in the ion trap formed by side chains of the Gln54 residues. The structure was rendered in PyMol from PDB 1VDF in ref. [32].

4.4 Viscoelastic Behavior of EPE L37A, EPE L37V, and EPE L37I Hydrogels

Sequence variation in the coiled-coil domain was further explored using EPE variants containing point mutations at leucine 37. Mutation of this residue to alanine by Gunasekar *et al*. resulted in a decrease in the helicity of the P domain from 70% in the wild-type to 22% in the mutant [28]. In hydrogels prepared by cross-linking EPE L37A with PEG-4VS, *G'* is independent of the oscillation frequency below approximately 5 rad s^{-1} but increases with increasing frequency beyond this value (Figure IV-8 a). A high frequency plateau is not observed in the experimental frequency range, which extends to 100 rad s^{-1}. The increase in *G'* is also accompanied by a local maximum in *G"*. As with the EPE variant containing the I58A mutation, the shift of the *G'* and

G" curves to higher frequencies relative to EPE suggests that transient physical cross-linking is still present, but significantly more dynamic. The relaxation time of the EPE L37A network, which is estimated as 0.06 s from the frequency at which the maximum in *G"* occurs and 0.02 s from the stress relaxation experiment (Figure IV-8 b and Table IV-4), is approximately three orders of magnitude less than the relaxation time in the EPE network. This effect is similar to the difference in the strand exchange time measured for leucine zipper peptides when single leucine to alanine substitutions were made (~1800 s to ~1) [24].

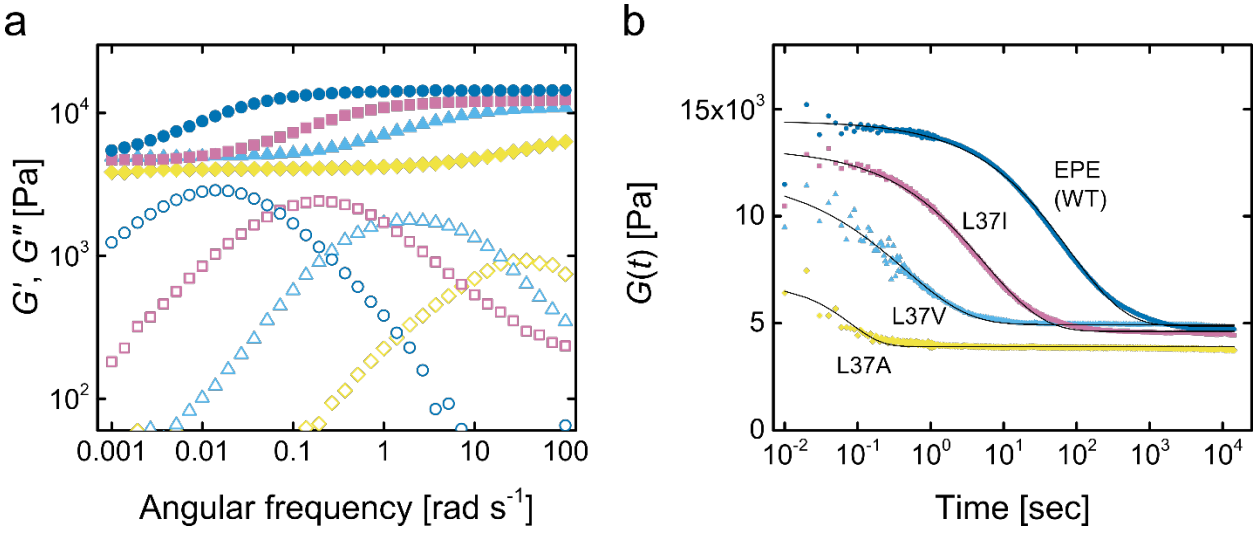

Figure IV-8. Rheology of EPE variants with point mutations at position 37 (EPE L37I, EPE L37V, and EPE L37A). (**a**) Dynamic oscillatory frequency sweeps showing the storage modulus, (*G'*, filled symbols) and loss modulus (*G"*, open symbols) at 2% strain amplitude, 25 °C. In gels prepared from the EPE L37I (squares), EPE L37V (triangles), and EPE L37A (diamonds) variants, the *G'* and *G"* curves are shifted to higher frequencies relative to EPE gels (circles). (**b**) The same trend is observed in stress relaxation experiments in which gels were subjected to a 2% step strain at 25 °C. The characteristic relaxation times were determined from the fitting the stretched exponential model for WT, L37I, and L37V (solid black lines). The relaxation function for EPE L37A was not well fit by the stretched exponential model, so the single exponential fit is shown instead. The trend in the characteristic relaxation time is $\tau_{WT} > \tau_{L37I} > \tau_{L37V} > \tau_{L37A}$.

The accessible surface area of the alanine side chain is approximately one-half that of the leucine side chain (67 $Å^2$ versus 137 $Å^2$) [36], and the loss of hydrophobic contacts at this position likely destabilizes the coiled-coil cross-linking and leads to faster network relaxation. Based on this hypothesis, EPE variants containing either the L37V or L37I mutation were also prepared. The accessible surface area of valine (117 $Å^2$) is between leucine and alanine. Isoleucine has an accessible surface area (140 $Å^2$) that is similar to leucine but its carbon atoms are arranged in a different branching structure [36]. In both EPE L37V and EPE L37I gels, the curves for *G'* and *G"* are shifted to higher frequencies relative to EPE gels, but the shift is not as large as observed in EPE L37A gels (Figure IV-8 a). The characteristic relaxation timescales for EPE L37V and EPE L37I networks are on the order of 1 s and 10 s, respectively (Figure IV-8 b and Table IV-4). These results establish a trend in the network relaxation time for EPE variants that differ by the identity of the side chain at position 37 (EPE L37 > EPE L37I > EPE L37V > EPE L37A), and demonstrate how rational design of the coiled-coil cross-linking domains can be used to program the relaxation behavior of chemical-physical hydrogels.

4.5 Disruption of Physical Cross-linking Under Denaturing Conditions

When hydrogels prepared from EPE and its variants are swollen in buffer containing 6 M guanidinium chloride as protein denaturant, the physical cross-links between the midblock domains are disrupted but the gels remain intact due to the covalent cross-links. The storage modulus of gels swollen in denaturing buffers is nearly independent of the oscillation frequency (Figure IV-9 a). This behavior is characteristic of covalent elastic networks. Hydrogels swollen in PBS with 6 M guanidinium chloride are also more swollen than hydrogels swollen in PBS (Figure IV-9 b), which is likely due to a combination of the loss of physical cross-linking and a more

extended conformation of protein chains. Because the association between the coils is absent under denaturing conditions, the proteins are nearly indistinguishable and the sequence variation no longer determines the macroscopic properties of the hydrogel.

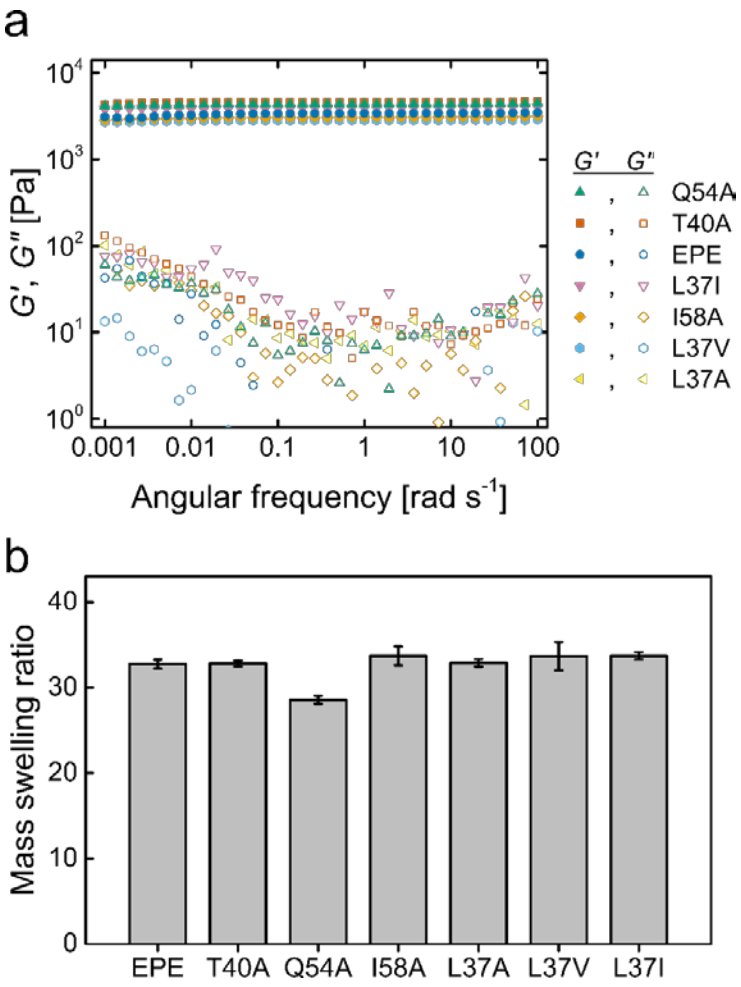

Figure IV-9. Rheology and swelling of EPE and EPE variants under denaturing conditions. (**a**) Hydrogels were swollen in PBS, pH 7.4 with 6 M guanidinium chloride. In frequency sweeps at 2% strain amplitude, 25 °C, the storage moduli are nearly independent of the oscillation frequency and the loss moduli do not exhibit local maxima. The rise in *G"* at low frequency (0.001-0.01 rad s^{-1}) may be due to slip. (**b**) Hydrogels swollen in PBS containing 6 M guanidinium chloride exhibit similar mass swelling ratios, with the exception of EPE Q54A, which is slightly less swollen than the other gels.

4.6 Chemical-Physical Protein Hydrogels with Multiple Relaxation Timescales

The approach developed here can be extended to design materials with more complex relaxation dynamics. In Chapter 3, hydrogels were prepared by cross-linking mixtures of EPE and a second artificial protein, ERE, that contains a non-associative midblock R in place of P. In these materials the amount of stress relaxation decreased as the amount of ERE was increased relative to EPE. The same approach was used to design a material that would exhibit two distinct relaxation timescales that are encoded by orthogonal coiled-coil cross-linkers. Shen *et al.* developed physical hydrogels from telechelic artificial proteins with two different helical endblocks that do not associate with one another [27]. The N-terminal block was the P domain used in this study, and the C-terminal block was a leucine zipper domain A that associates to form homotetrameric coiled coils (Figure IV-10 a). This topology successfully decreased the erosion rate by suppressing the formation of loops, but the individual relaxation times of the two coiled coils were not observed. One explanation is that the relaxation timescales for P coiled coils and A coiled coils in these gels are too similar to observe in SAOS frequency sweep experiments. More likely, however, is that once the faster relaxing domain dissociates, the proteins are no longer connected to the network and behave instead as 8- or 10-arm star polymers until the second relaxation time is reached.

It should be possible to observe two distinct relaxation timescales in chemical-physical networks by cross-linking a mixture of proteins that meet two criteria. First, the proteins must have orthogonal physical cross-linking domains, and second, the relaxation timescales for these domains must be sufficiently separated. In a SAOS frequency sweep experiment, these materials would be expected to exhibit three plateaus in the storage modulus and two local maxima in the loss modulus. The first plateau would correspond to high frequencies or timescales that are shorter than the dissociation times of both physical cross-linkers. A second plateau at intermediate

frequencies or timescales would occur once the chain segments cross-linked by the fast dissociating cross-linker relax. Finally, the low frequency plateau would correspond to the stress stored between the chemical cross-links at timescales greater than the dissociation times of both physical cross-linkers.

To construct such a network, an artificial protein EAE was designed in which the P domain was replaced with the A leucince zipper. Hydrogels prepared from EAE exhibit relaxation behavior (Figure IV-10 c and d) that is similar to one of more stable EPE variants, EPE Q54A. The mean relaxation time for the EAE network is approximately 1200 s, consistent with measurements of the strand exchange time for A measured by Shen *et al*. [18]. This suggests that physical cross-links formed by the A domain have a longer average lifetime than physical cross-links formed by the P domain. To enhance this difference and meet the two criteria for observing multiple relaxation timescales, EAE was paired with EPE L37V within the same covalent network (Figure IV-10 b, iv). The single leucine to valine point mutation in P is not expected to affect its orthogonality with A, and the relaxation times of the individual EAE and EPE L37V networks are separated by approximately three orders of magnitude. Hydrogels were prepared by cross-linking a mixture containing equal amounts of EAE and EPE L37V under denaturing conditions followed by swelling to equilibrium in PBS, pH 7.4. In both SAOS frequency sweep experiments and stress relaxation experiments (Figure IV-10 c and d and Figure IV-12 a), two relaxation timescales are present that correspond to the relaxation timescales observed in EPE L37V and EAE single protein networks. These relaxations represent the transition from a high frequency/short time plateau to an intermediate frequency/intermediate time plateau, and from the intermediate frequency/intermediate time plateau to the low frequency/long time plateau, respectively. As expected, the frequencies at which the transitions between these plateaus occur correspond to the

frequencies at which local maxima in *G"* occur. Notably, a local minimum in *G"* in the EPE L37V:EAE gel occurs near the intersection of the *G"* curves of the individual EPE L37V and EAE gels.

The stress relaxation function, $G(t)$, was fit by a double stretched exponential model,

$$G(t) = G_1 \exp\left(-\left(\frac{t}{\tau_{L37V}}\right)^{\beta_{L37V}}\right) + G_2 \exp\left(-\left(\frac{t}{\tau_{EAE}}\right)^{\beta_{EAE}}\right) + G_e \qquad \text{(Equation IV-3)}$$

which contains two exponential terms identical to those observed in Eq. IV-1 and an equilibrium modulus G_e representing the chemical cross-linking. To fit the experimental $G(t)$ data for the EPE L37V:EAE network, the characteristic relaxation timescales (τ_{L37V} and τ_{EAE}) and the stretching exponents (β_{L37V} and β_{EAE}) were fixed at the values determined from the EPE L37V and EAE single protein networks, leaving G_1, G_2, and G_e as adjustable parameters. This assumes that the exchange rate of P L37V and A coiled coils in the EPE L37V:EAE mixed protein network is the same as the exchange rate in the single protein networks, which appears to be the case based on the frequency sweep experiments (Figure IV-10 e and d). As shown in Figure IV-12 a, the double stretched exponential model provides a good fit of the experimental data.

The same material design was employed to prepare chemical-physical hydrogel networks from a mixture of proteins that are not expected to exhibit orthogonal physical cross-linking (Figure IV-10 b, v). While the relaxation timescales in single protein networks prepared from EPE L37V and EPE Q54A are separated by several orders of magnitude, mixed species physical cross-linkers are expected to form in a network prepared from an equimolar mixture of the two proteins. In this network, six combinations of strands are possible assuming pentameric association of the midblock domains. While these six combinations are expected to have six different relaxation

times that lie between the fastest combination (all strands from EPE L37V) and the slowest combination (all strands from EPE Q54A), the equilibrium distribution of these combinations is not known *a priori*. Frequency sweep and stress relaxation experiments of EPE L37V:EPE Q54A gels reveal a much broader relaxation than was observed with EAE:EPE L37V gels, consistent with several relaxation timescales (Figure IV-10 e and f and Figure IV-12 b). Unlike the EPE L37V:EAE network, the EPE L37V:EPE Q54A network is not well fit by the double stretched exponential model, suggesting that several relaxation timescales are present and that additional terms are needed to adequately model the experimental data.

It is also noted that a decrease in *G'* and an increase in *G"* are observed near an angular frequency of 0.001 rad s^{-1} in EPE Q54A:EPE L37V gels. These features occur near the characteristic relaxation timescale expected for P Q54A physical cross-links. This suggests that a significant number of homotypic P Q54A cross-links are present in this gel, which is not surprising given that EPE Q54A is expected to have a higher fraction of folded midblock domains than EPE L37V. These experiments demonstrate that multiple relaxation timescales can be programmed in chemical-physical protein networks, and that the use of orthogonal coiled-coil domains as physical cross-linkers allows two distinct relaxation timescales to be observed.

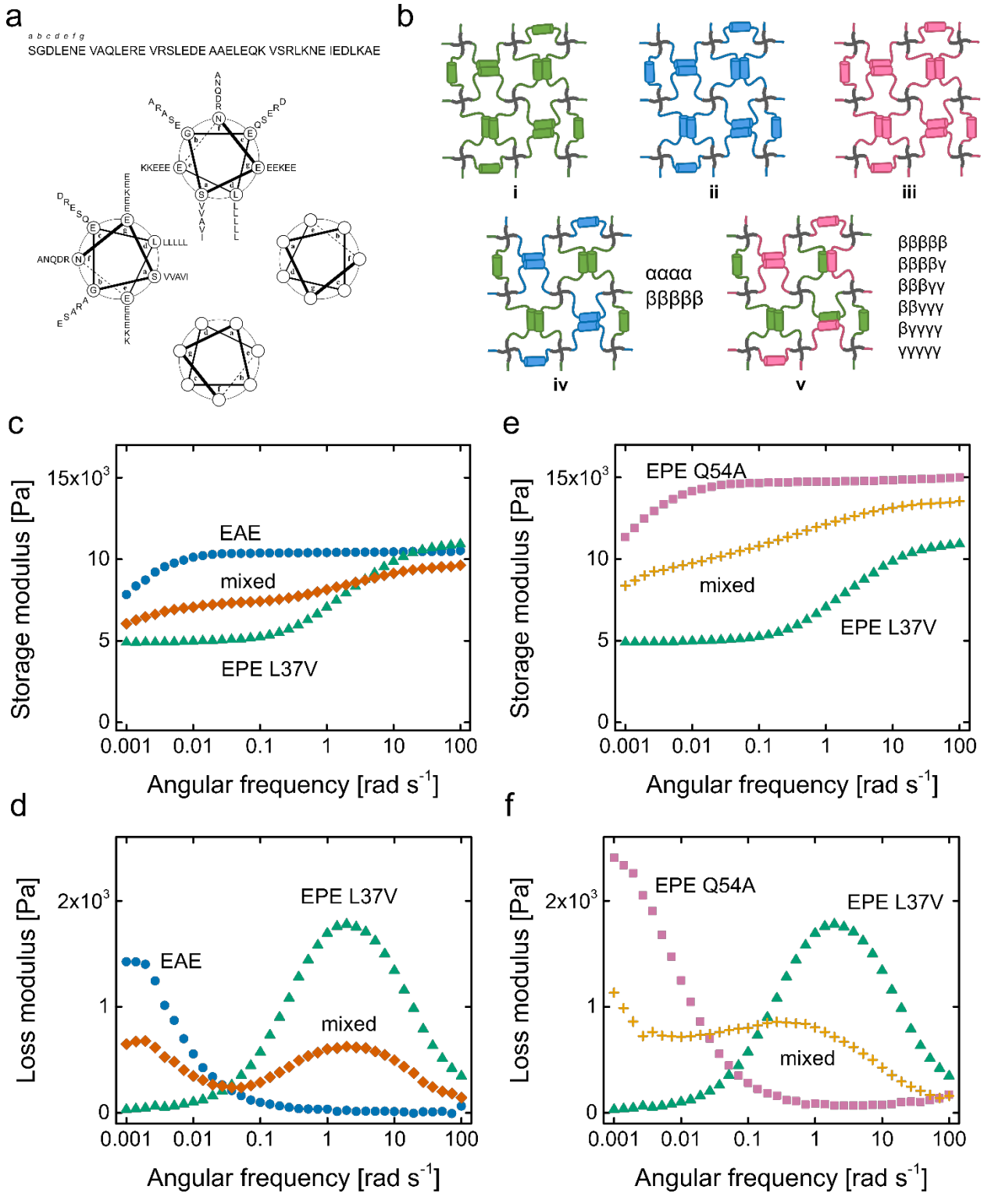
a
b
i
ii
iii
iv
v
αααα
ββββββ
βββββ
ββββγ
βββγγ
ββγγγ
βγγγγ
γγγγγ
c
e
d
f
Storage modulus [Pa]
Loss modulus [Pa]
Angular frequency [rad s-1]
EAE
mixed
EPE L37V
EPE Q54A
15x10^3
2x10^3
0.001
0.01
0.1
1
10
100

Figure IV-10 (previous page). Chemical-physical protein networks with multiple relaxation timescales. (**a**) Sequence of the A leucine zipper protein domain and helical wheel representation of a parallel A homotetramer (antiparallel orientations are also possible). (**b**) Schematic representation of chemical-physical protein networks prepared from a single artificial protein (i. EPE L37V, ii. EAE, iii. EPE Q54A) or two artificial proteins with different associative midblocks (iv. EPE L37V:EAE, v. EPE L37V:EPE Q54A). In network iv, the coiled coils are orthogonal to one another and two types of physical cross-links are present, tetramers composed of α and pentamers composed of β. In network v, mixed species cross-linking is possible, leading to six different pentamers of β and γ. (**c**) Storage modulus and (**d**) loss modulus of EAE gels (circles), EPE L37V gels (triangles), and gels prepared by cross-linking an equimolar mixture of EAE and EPE L37V (diamonds). (**e**) Storage modulus and (**f**) loss modulus of EPE Q54A gels (squares), EPE L37V gels (up triangles), and gels prepared by cross-linking an equimolar mixture of EPE Q54A and EPE L37V (crosses).

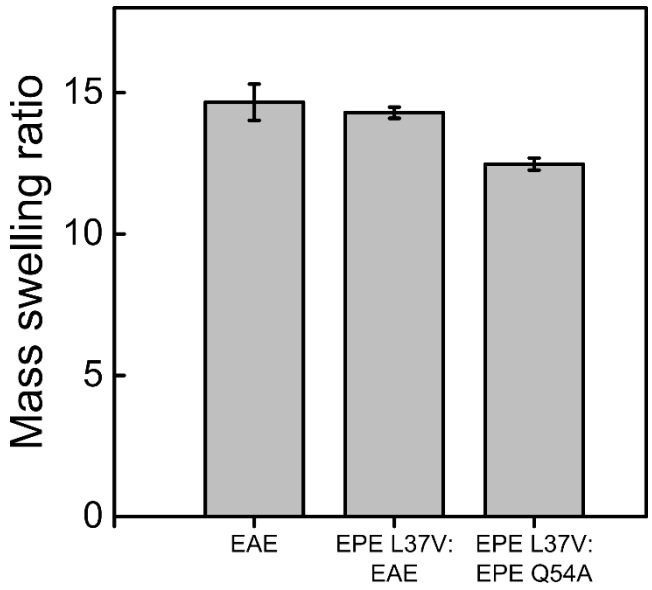

Figure IV-11. Equilibrium mass swelling ratio of EAE gels and mixed protein networks. The mass swelling ratios of the EAE single protein network and EPE L37V:EAE and EPE L37V:EPE Q54A mixed protein networks swollen in PBS, pH 7.4, room temperature.

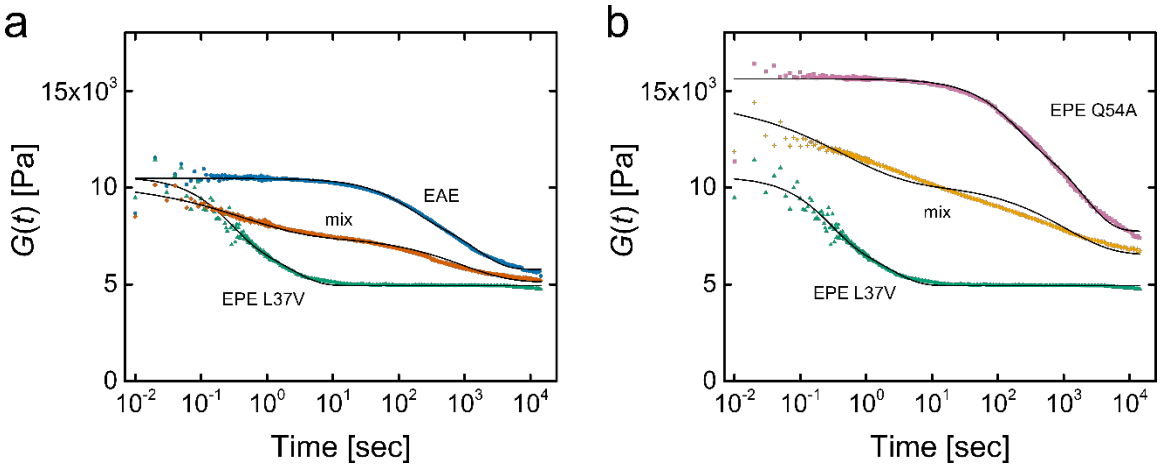

Figure IV-12. Stress relaxation of EPE L37V:EAE and EPE L37V:EPE Q54A mixed composition gels. (**a**) The relaxation function $G(t)$ is plotted for single protein networks EPE L37V and EAE and the mixed protein network EPE L37V:EAE. (**b**) $G(t)$ was also plotted for the EPE Q54A single protein network and the EPE L37V:EPE Q54A mixed protein network. The solid lines are fits of the stretched exponential model (Eq. IV-1) for single protein networks and a double stretched exponential model (Eq. IV-3) for mixed protein networks. The double stretched exponential model is well fit by the EPE L37V:EAE network, which contains an orthogonal pair of physical cross-linking domains, but not EPE L37V:EPE Q54A.

5. Conclusions

The sequence-structure-function paradigm has guided our understanding of how protein structure and function are encoded in an amino acid sequence as well as efforts to predict protein function and to design new proteins. The same paradigm can be applied to designing sequences of artificial proteins in order to encode the macroscopic behavior of protein-based materials. Here, sequence variation within the physical cross-linking domain of an artificial protein was used to engineer the dynamic behavior of protein networks. Single point mutations within a helical domain that forms coiled-coil cross-links resulted in variations of the characteristic relaxation timescale over five orders of magnitude. Networks prepared from mixtures of artificial proteins containing two different physical cross-linking domains exhibited more complex dynamic behavior and are capable of stress relaxation and energy dissipation on multiple timescales. Dynamic materials might play important roles in regulating or directing cell and tissue behavior [6-8, 37-39]. They also exhibit enhancements in toughness and extensibility that is related to their ability to dissipate energy when deformed [40]. The ability to program relaxation behavior in networks consisting of a single artificial protein or multiple artificial proteins will have important applications in these areas and others.

6. References

[1] H.-B. Wang, M. Dembo, Y.-L. Wang *Am. J. Physiol. - Cell Ph.* **2000** *279*, C1345-C1350.

[2] R.J. Pelham, Y.-l. Wang *Proc. Natl. Acad. Sci. USA* **1997** *94*, 13661-13665.

[3] A.J. Engler, S. Sen, H.L. Sweeney, D.E. Discher *Cell* **2006** *126*, 677-689.

[4] S.S. Soofi, J.A. Last, S.J. Liliensiek, P.F. Nealey, and C.J. Murphy *J. Struct. Biol.* **2009** *167*, 216-219.

[5] M.F. Ashby, *Materials Selection in Mechanical Design* Elsevier Butterworth-Heinemann, Amsterdam **2005**.

[6] A.R. Cameron, J.E. Frith, J.J. Cooper-White *Biomaterials* **2011** *32*, 5979-5993.

[7] O. Chaudhuri, L. Gu, M. Darnell, D. Klumpers, S.A. Bencherif, J.C. Weaver, N. Huebsch, and D.J. Mooney *Nat. Commun.* **2015** *6*.

[8] M. Murrell, R. Kamm, P. Matsudaira *Biophys J.* **2011** *101*, 297-306.

[9] T. Annable, R. Buscall, R. Ettelaie, D. Whittlestone *J. Rheol.* **1993** *37*, 695-726.

[10] R.P. Sijbesma, F.H. Beijer, L. Brunsveld, B.J.B. Folmer, J.H.K.K. Hirschberg, R.F.M. Lange, J.K.L. Lowe, and E.W. Meijer *Science* **1997** *278*, 1601-1604.

[11] D.E. Fullenkamp, L. He, D.G. Barrett, W.R. Burghardt, and P.B. Messersmith *Macromolecules* **2013** *46*, 1167-1174.

[12] M.S. Menyo, C.J. Hawker, J.H. Waite *ACS Macro Lett.* **2015** *4*, 1200-1204.

[13] S.C. Grindy, R. Learsch, D. Mozhdehi, J. Cheng, D.G. Barrett, Z. Guan, P.B. Messersmith, and N. Holten-Andersen *Nat. Mater.* **2015** *14*, 1210-1216.

[14] D.M. Loveless, S.L. Jeon, S.L. Craig *Macromolecules* **2005** *38*, 10171-10177.

[15] D.D. McKinnon, D.W. Domaille, J.N. Cha, K.S. Anseth *Adv. Mater.* **2014** *26*, 865-872.

[16] H. Ying, Y. Zhang, J. Cheng *Nat. Commun.* **2014** *5*.

[17] W.A. Petka, J.L. Harden, K.P. McGrath, D. Wirtz, and D.A. Tirrell *Science* **1998** *281*, 389-392.

[18] W. Shen, J.A. Kornfield, D.A. Tirrell *Macromolecules* **2007** *40*, 689-692.

[19] S. Tang, M. Wang, B.D. Olsen *J. Am. Chem. Soc.* **2015** *137*, 3946-3957.

[20] C. Xu, V. Breedveld, J. Kopeček *Biomacromolecules* **2005** *6*, 1739-1749.

[21] P.J. Skrzeszewska, F.A. de Wolf, M.W.T. Werten, A.P.H.A. Moers, M.A. Cohen Stuart, and J. van der Gucht *Soft Matter* **2009** *5*, 2057-2062.

[22] S. Ozeki, T. Kato, M.E. Holtzer, A. Holtzer *Biopolymers* **1991** *31*, 957-966.

[23] S.-Y. Park, C.M. Quezada, A.M. Bilwes, B.R. Crane *Biochemistry* **2004** *43*, 2228-2240.

[24] H. Wendt, C. Berger, A. Baici, R.M. Thomas, and H.R. Bosshard *Biochemistry* **1995** *34*, 4097-4107.

[25] L.R. Patel, T. Curran, T.K. Kerppola *Proc. Natl. Acad. Sci. USA* **1994** *91*, 7360-7364.

[26] V.P. Efimov, A. Lustig, J. Engel *FEBS Lett.* **1994** *341*, 54-58.

[27] W. Shen, K. Zhang, J.A. Kornfield, D.A. Tirrell *Nat. Mater.* **2006** *5*, 153-158.

[28] S.K. Gunasekar, M. Asnani, C. Limbad, J.S. Haghpanah, W. Hom, H. Barra, S. Nanda, M. Lu, and J.K. Montclare *Biochemistry* **2009** *48*, 8559-8567.

[29] A.V. Terskikh, S.A. Potekhin, T.N. Melnik, A.V. Kajava *Lett. Pept. Sci.* **1997** *4*, 297-304.

[30] Y. Guo, R.A. Kammerer, J. Engel *Biophys. Chem.* **2000** *85*, 179-186.

[31] G.L. Ellman *Arch. Biochem. Biophys.* **1959** *82*, 70-77.

[32] V.N. Malashkevich, R.A. Kammerer, V.P. Efimov, T. Schulthess, and J. Engel *Science* **1996** *274*, 761-765.

[33] Y. Guo, D. Bozic, V.N. Malashkevich, R.A. Kammerer, T. Schulthess, and J. Engel *EMBO J.* **1998** *17*, 5265-5272.

[34] A.A. MacFarlane, G. Orriss, N. Okun, M. Meier, T. Klonisch, M. Khajehpour, and J. Stetefeld *PLOS One* **2012** *7*, e48130.

[35] S. Özbek, J. Engel, J. Stetefeld *EMBO J.* **2002** *21*, 5960-5968.

[36] S. Miller, J. Janin, A.M. Lesk, C. Chothia *J. Mol. Biol.* **1987** *196*, 641-656.

[37] Y. Liu, B. Liu, J.J. Riesberg, W. Shen *Macromol. Biosci.* **2011** *11*, 1325-1330.

[38] D.D. McKinnon, D.W. Domaille, T.E. Brown, K.A. Kyburz, E. Kiyotake, J.N. Cha, and K.S. Anseth *Soft Matter* **2014** *10*, 9230-9236.

[39] H. Wang, S.C. Heilshorn *Adv. Mater.* **2015** *27*, 3717-3736.

[40] X. Zhao *Soft Matter* **2014** *10*, 672-687.